JACS
JOURNAL OF THE AMERICAN CHEMICAL SOCIETY
Article
pubs.acs.org/JACS

Converting a Light-Driven Proton Pump into a Light-Gated Proton Channel

Keiichi Inoue,[†,‡,§] Takashi Tsukamoto,[∥] Kazumi Shimono,[⊥] Yuto Suzuki,[†] Seiji Miyauchi,[⊥] Shigehiko Hayashi,[#] Hideki Kandori,[†,‡] and Yuki Sudo*[,∥,▽]

[†]Department of Frontier Materials, Nagoya Institute of Technology, Showa-ku, Nagoya 466-8555, Japan
[‡]OptoBioTechnology Research Center, Nagoya Institute of Technology, Showa-ku, Nagoya 466-8555, Japan
[§]PRESTO, Japan Science and Technology Agency, 4-1-8 Honcho Kawaguchi, Saitama 332-0012, Japan
[∥]Division of Pharmaceutical Sciences, Graduate School of Medicine, Dentistry, and Pharmaceutical Sciences, Okayama University, 1-1-1 Tsushima-naka, Kita-ku, Okayama 700-8530, Japan
[⊥]Faculty of Pharmaceutical Sciences, Toho University, Funabashi 274-8510, Japan
[#]Department of Chemistry, Graduate School of Science, Kyoto University, Kyoto 606-8502, Japan
[▽]Japan Science and Technology Agency, CREST, K's Gobancho, 7 Gobancho, Chiyoda-ku, Tokyo 102-0076, Japan

Supporting Information

ABSTRACT: There are two types of membrane-embedded ion transport machineries in nature. The ion pumps generate electrochemical potential by energy-coupled active ion transportation, while the ion channels produce action potential by stimulus-dependent passive ion transportation. About 80% of the amino acid residues of the light-driven proton pump archaerhodopsin-3 (AR3) and the light-gated cation channel channelrhodopsin (ChR) differ although they share the close similarity in architecture. Therefore, the question arises: How can these proteins function differently? The absorption maxima of ion pumps are red-shifted about 30−100 nm compared with ChRs, implying a structural difference in the retinal binding cavity. To modify the cavity, a blue-shifted AR3 named AR3-T was produced by replacing three residues located around the retinal (i.e., M128A, G132V, and A225T). AR3-T showed an inward H^+ flux across the membrane, raising the possibility that it works as an inward H^+ pump or an H^+ channel. Electrophysiological experiments showed that the reverse membrane potential was nearly zero, indicating light-gated ion channeling activity of AR3-T. Spectroscopic characterization of AR3-T revealed similar photochemical properties to some of ChRs, including an all-*trans* retinal configuration, a strong hydrogen bond between the protonated retinal Schiff base and its counterion, and a slow photocycle. From these results, we concluded that the functional determinant in the H^+ transporters is localized at the center of the membrane-spanning domain, but not in the cytoplasmic and extracellular domains.

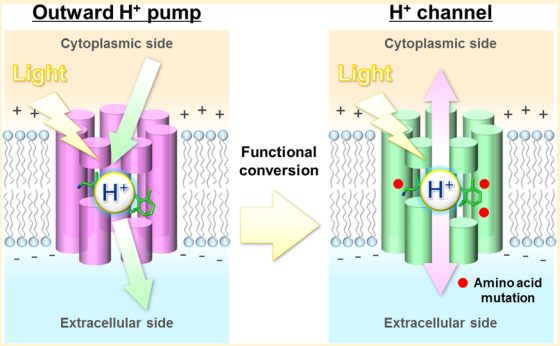

INTRODUCTION

The activities of organisms are maintained by an electrochemical membrane potential which refers to ion gradients across the cellular membrane. The membrane potential is generated by energy-coupled ion pumps and transiently dissipated by stimulus-induced ion channels. Molecular and evolutionary aspects of both types of ion transporter machineries are therefore of interest for many researchers. Microbial rhodopsins are photoreceptive hepta-transmembrane proteins found in various microorganisms such as eubacteria, archaea, and fungi.[1] Most of them share a common chromophore, all-*trans* retinal (ATR), which covalently binds to a conserved Lys residue on the seventh helix through a Schiff base linkage, and it isomerizes to the 13-*cis* form by visible light absorption. Retinal isomerization evokes subsequent conformational changes of the protein, and a variety of biological functions arise during the photochemical reaction. Although the microbial rhodopsins show seemingly dissimilar functions [e.g., outward proton (H^+) and sodium ion (Na^+) pumps,[2−4] inward chloride (Cl^-) pumps,[5,6] positive- and negative-phototaxis sensors,[7−9] light-gated cation channels[10,11] and regulation of gene expression[12]], their basic function is roughly divided into ion transport and signaling[1] (Figure 1a). A light-driven H^+ pump bacteriorhodopsin (BR) was discovered from the halophilic archaeon *Halobacterium salinarum* in 1971.[1] BR generates H^+ gradients across the membrane, resulting in ATP synthesis by collaborating with an enzyme ATP synthase. Abundance of protein in the native membrane and its high stability allowed one to investigate the molecular mechanism of

Received: November 17, 2014
Published: February 25, 2015

DOI: 10.1021/ja511788f
J. Am. Chem. Soc. 2015, 137, 3291−3299

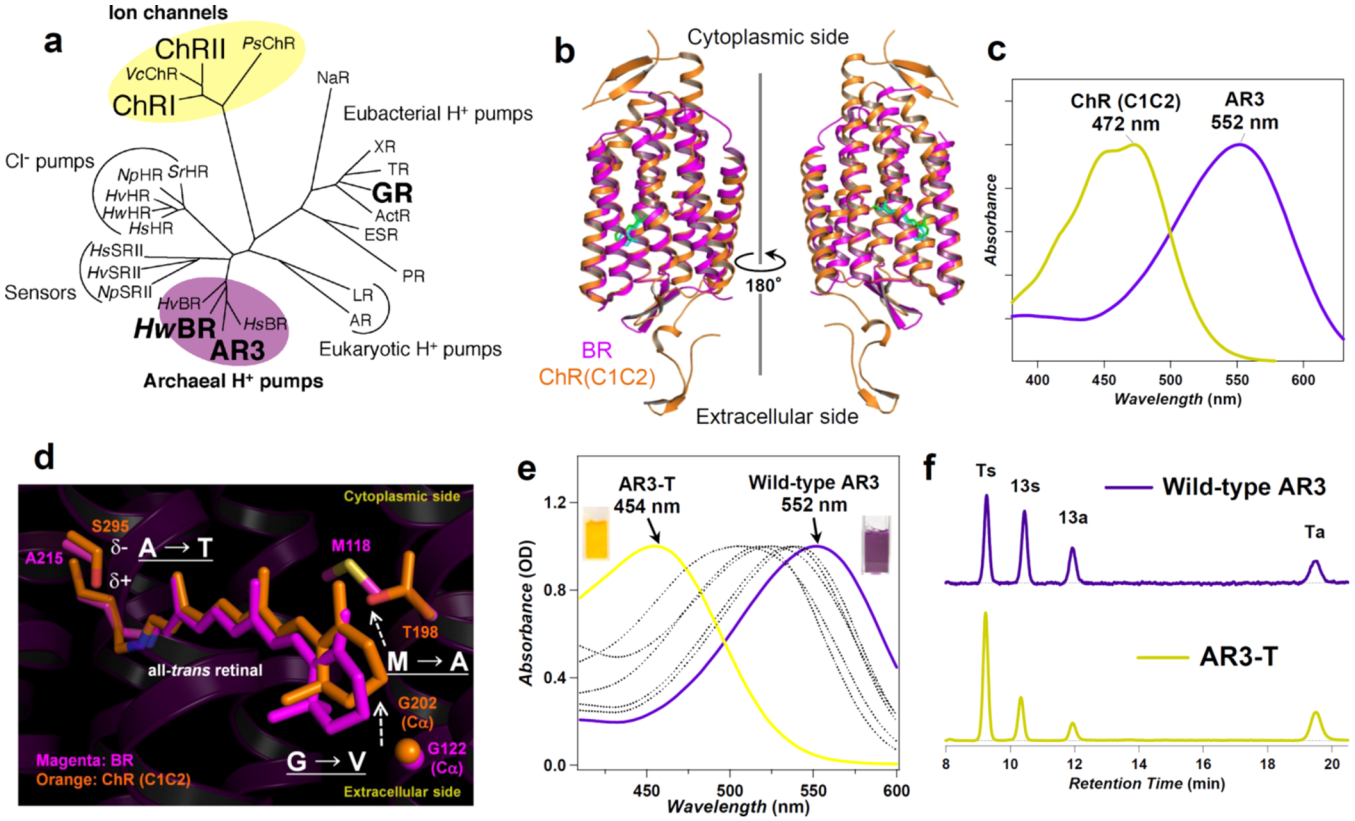

Figure 1. Light-driven ion pumps versus light-gated ion channels. (a) Phylogenic tree of microbial rhodopsins. The H^+ pumps studied here are indicated by bold characters. (b) Crystal structures of BR (PDB code: 1C3W, purple)[13] and a chimeric protein of ChR (C1C2, PDB code: 3UG9, orange).[14] (c) Absorption spectra of AR3 and ChR (C1C2).[15] (d) Structure of the retinal binding site of BR (1C3W, purple) and C1C2 (orange). (e) Absorption spectra of wild-type AR3 (purple) and AR3-T (yellow). Spectra of M128A, G132V, A225T, M128A/A225T, and G132 V/A225T are shown by dashed black lines. (f) Chromophore configurations extracted from wild-type AR3 and AR3-T. The detection beam was set to 360 nm. Ts, Ta, 13s, and 13a stand for all-*trans*-15-*syn*, all-*trans*-15-*anti*, 13-*cis*-15-*syn*, and 13-*cis*-15-*anti* retinal oxime, respectively. The molar composition of each retinal isomer was calculated from the areas of the peaks in the HPLC patterns, and the estimated compositions of all-*trans* configuration are listed in Table 1.

ion transport in detail. After 2000, genomic analysis revealed that BR-like H^+ pumps are widely distributed among different taxa, including members of the domain bacteria and eukaryotes (Figure 1a), indicating that many organisms generate biochemical energy ATP from light.[16] In addition to the "pump", in 2002 and 2003, light-gated passive cation channels named channelrhodopsin (ChR, channelrhodopsin-1; ChR1 and channelrhodopsin-2; ChR2) were discovered in the eukaryote *Chlamydomonas reinhardtii*.[10,11] The ChRs are responsible for changes in motility responses through membrane depolarization by ion channeling activity upon photoillumination.[17,18] After the discoveries, these ion transport machineries are biotechnologically utilized as a molecular switch for controlling the neural activity by light.[19] In a new technology named optogenetics, light-driven H^+ and Cl^- pumps are used as optical silencers of neuronal activity,[20,21] while ChRs excite the neurons by cation influx upon photoillumination.[19] Various functional improvements as optogenetic tools were achieved by protein engineering, and recently functional conversions from the cation channel to the anion ones have been reported.[22,23] Thus, in addition to its biological significance, ion-transporting rhodopsins have become a focus of interest in part because of their importance to rational design and engineering of photoswitchable molecules.

Although approximately 74−84% of the amino acid residues of H^+ pumps and ChRs differ,[1] they show close similarities in architecture in terms of helix positions and locations of retinal-binding cavity (Figure 1b). Here, it is curious to understand how these proteins function differently. In general, functional conversion by protein engineering provides critical information about molecular and evolutionary aspects of biological molecules. Among retinal proteins, in 1995, the conversion of an H^+ pump BR to a Cl^- pump was achieved by only mutating an aspartate of BR, which is a primary counterion of the retinal protonated Schiff base, to a serine or a threonine.[24] This implied that the determinant of ion selectivity is localized around the Schiff base region. In 2006, it was reported that replacement of three hydrogen-bonding residues converts an H^+ pump BR into a sensory receptor.[25] This demonstrated that evolution accomplished an elegant but simple conversion and that essential differences between transport proteins and signaling ones in the rhodopsin family are far less than previously imagined.

In this study, we attempted to convert a BR-like H^+ pump archaerhodopsin-3 (AR3) into a ChR-like ion channel. As described above, the tertiary structures of microbial rhodopsins are very similar (Figure 1b), suggesting that functional differentiation is achieved by considerably small differences. Thus, it is expected that functional conversion by mutagenesis is possible without extensive substitution of amino acid

DOI: 10.1021/ja511788f
J. Am. Chem. Soc. 2015, 137, 3291−3299

residues. A guide for design of the conversion is the notable differences in the absorption maxima between ion pumps and ion channels. As shown in Figure 1c, the absorption maxima of ion pumps are red-shifted about 30−100 nm relative to ion channels, suggesting a significant structural difference in the retinal chromophore between them. In fact, the chromophore structure of the H^+ pump BR is significantly different from that of the chimera of ChR1 and ChR2 (C1C2), especially around the β-ionone ring (Figure 1d). Compared to BR, the β-ionone ring of C1C2 moved to the cytoplasmic side (Figure 1d). We hypothesized that the structural difference of retinal in two types of ion transport machineries causes functional differentiation, and simultaneously color changes between them. To verify this, in this study, three mutations were introduced into AR3. Two of them were expected to induce the movement of the β-ionone ring toward the cytoplasmic side by introduction of smaller (M → A) and larger (G → V) residues on the cytoplasmic and extracellular sides, respectively (Figure 1d). One mutation is for a hydrophobic residue Ala located in the vicinity of the Schiff base (A → T), which is a key residue for color tuning in a variety of microbial rhodopsins such as BR, sensory rhodopsin I (SRI), sensory rhodopsin II (SRII), and middle rhodopsin (MR).[25−28] The A to T mutation is therefore expected to alter the chromophore structure as well (Figure 1d). Thus, the mutations on three amino acid residues in AR3 are expected to optimize the structure of the retinal binding cavity, which can be monitored by measuring absorption spectra. The atomistically detailed design principle to create the blue-shifted photoabsorption will be reported elsewhere.

MATERIALS AND METHODS

Sample Preparation. The expression plasmids for wild-type AR3, *Hw*BR, and GR were constructed as described previously.[29,30] The mutant genes were constructed by the QuikChange site-directed mutagenesis method as described previously.[26] All constructed plasmids were analyzed using an automated sequencer to confirm the expected nucleotide sequences. The *E. coli* strains, DH5α and BL21(DE3), were used as hosts for DNA manipulation and for protein expression of the histidine-tagged proteins, respectively. The crude membrane was solubilized by a detergent *n*-dodecyl-β-D-maltoside (DDM, Dojindo, Japan), and the solubilized fraction was purified by Ni^{2+} affinity column chromatography. Where necessary, samples were further purified with an anion exchange column.

Ion Transport Activity. *E. coli* cells were washed and resuspended in 100 mM NaCl solution. The light-induced pH change was monitored by a pH electrode. The light of wavelengths <20 nm shorter than λ_{max} was removed by a long-pass filter. To obtain action spectra, interference filters (fwhm = 10−15 nm) were used to obtain light at specific wavelengths by filtering the output of the same Xe arc lamp. The photon-flux of light was measured by a calibrated multichannel detector (IRRAD-C2000+, Ocean Optics), and the initial slopes at a specific wavelength were scaled by fluxes to obtain an action spectrum. Electrophysiological experiments in *Xenopus laevis* oocytes were performed using the two-electrode voltage-clamp technique described previously.[31] Briefly, the amplified cDNA was heterologously expressed in oocytes by cRNA injection. The oocytes were used for electrophysiological studies 3−5 days after cRNA injection. Then they were superfused with perfusion buffer (96 mM NaCl, 2 mM KCl, 1 mM $MgCl_2$, 1 mM $CaCl_2$, 10 mM HEPES, and 6 mM Tris, pH 7.5). The current−voltage (I−V) relationship was analyzed before and at 1 min after illumination with cyan light (peak wavelength, 505 nm) generated from a light-emitting diode (Luxeon V Star LXHL-LE5C, Lumileds Lighting Co., San Jose, CA). The measurements at different membrane potentials (−150 mV to +50 mV in 20-mV increments) were made using short pulses (100 ms).

Spectroscopic Analysis. Retinal composition was determined by HPLC as described previously.[32] Each sample was dark-adapted for several days before analysis. The pH titration experiments were performed using essentially the same method described previously.[30] In short, the absorbance of samples was approximately 0.5 optical densities at each absorption maximum. The samples were initially suspended in 50 mM Tris-HCl buffer (pH 7.0) containing 1 M NaCl and 0.05% DDM. Then, the pH was adjusted to the desired values by the addition of HCl and NaOH. Data showing the reversibility of spectral changes were used. For the data analysis, peaks of the difference spectra at 624 nm for the wild-type AR3 and 524 nm for AR3-T were plotted against pH and fitted by the Henderson−Hasselbalch equation with a single pK_a.

Transient absorption spectra were obtained by a flash photolysis system, using a multichannel detector (Hamamatsu Photonics K. K., Japan) as described previously.[4] Because purified AR3-T in DDM micelles significantly lost its color upon illumination, the *E. coli* membrane containing wild-type AR3 or AR3-T was used for the measurements. The cells were washed in a 1 M NaCl, 50 mM Tris-HCl (pH 7.0) solution and disrupted by sonication. Upon measurement, the sample was excited with a beam from an OPO system (LT-2214, LOTIS TII, Minsk, Republic of Belarus) produced by the third harmonics of a nanosecond pulsed Nd^{3+}-YAG laser (λ = 355 nm, LS-2134UTF, LOTIS TII, Minsk, Republic of Belarus). The laser power was 3 mJ per pulse.

The interval between laser pulses was 500 ms and 6 s for wild-type AR3 and AR3-T, respectively, which is sufficiently slower than their photocycles. Intensities of the transmitted probe light from a Xe lamp (L8004, Hamamatsu Photonics K. K.) were measured before and after sample excitation and transient absorption spectra were obtained by calculating the ratio between them. There were 100 spectra averaged to improve the signal-to-noise ratio.

Low-temperature Fourier transform infrared (FTIR) spectroscopy at 77 K was performed as described previously.[33−35] After hydration with H_2O or D_2O, samples reconstituted into L-α-phosphatidylcholine lipids (AR3: PC molar ratio of 1:50) were placed in a cell in a cryostat (DN-1704, Oxford Instruments, U.K.) mounted in an FTIR spectrometer (FTS-40, Agilent Technology). The cryostat was connected to a temperature controller (ITC-4, Oxford Instruments), and temperature was regulated with 0.1 K precision. For wild-type AR3, illumination with 500 nm light (KL-52, Toshiba, Tokyo, Japan) from a 1 kW halogen tungsten lamp at 77 K for 2 min converted AR3 to the K-intermediate, and subsequent illumination with >610 nm light (R-63, Toshiba, Tokyo, Japan) for 1 min reverted K back to AR3, as evidenced by the identical (but inverted) spectral shape. For AR3-T, the sample was illuminated with 440 nm light (KL-44, Toshiba, Tokyo, Japan) for 2 min, converting AR3-T to the K-intermediate. Then, K was reconverted to the initial state upon illumination with >520 nm light (O-54, Toshiba) for 1 min. The difference spectrum was calculated from the two spectra constructed from 128 interferograms taken before and after illumination. The 128 difference spectra, both obtained in this way, were averaged to produce each K minus AR3 spectrum.

RESULTS

Color Tuning. The absorption spectra of purified wild-type AR3 and its mutants are shown in Figure 1e. The absorption maxima (λ_{max}) are blue-shifted in a mutation-dependent manner. As expected, the AR3 triple mutant (M128A/G132V/A225T; abbreviated as AR3-T hereafter) showed a large blue-shifted λ_{max} of 454 nm, which is close to that of C1C2 (~472 nm) (see Figure 1c), suggesting that the chromophore structure of AR3-T is similar to that of C1C2. To investigate this, the composition of the retinal isomers of AR3-T was determined by high performance liquid chromatography (HPLC) experiments. It has been reported that archaeal H^+ pumps, including BR and AR3, possess approximately 50% ATR as a chromophore, while ChRs possess approximately

DOI: 10.1021/ja511788f
J. Am. Chem. Soc. 2015, 137, 3291−3299

Table 1. Photochemical and Structural Properties of Bacteriorhodopsin (BR), Wild-Type AR3, AR3-T, ChR1, ChR2, and Its Chimera (C1C2)

opsin type	λ_{max} [nm]	ion flux	pK_a of the counterion	ATR [%]	C=N stretch (cm^{-1})	photocycling rate [s]
BR	570	pump	2.7[a]	~47[b]	1641 (Δ13 cm^{-1})	~0.01
AR3	552	pump	3.0	53 ± 2[c]	1642 (Δ15 cm^{-1})	~0.05
AR3-T (M128A/G132V/A225T)	454	channel	3.9	65 ± 3	1662 (Δ30 cm^{-1})	~30
ChR1	519[d]	channel	~9[d]	71[e]	1646[e] (Δ23 cm^{-1})	25[f]
ChR2	465	channel	n.d.[j]	70[g]	1657 (Δ28 cm^{-1})	~20[h]
C1C2	472	channel	5.8[i]	n.d.	1665 (Δ29 cm^{-1})	n.d.

[a]From Brown et al. *Biophys. J.* **1993**.[42] [b]From Petti et al. *Biochemistry* **1977**. [c]From Sudo et al. *J. Biol. Chem.* **2013**. [d]From Li et al. *Biophys. J.* **2014**. [e]Muders et al. *FEBS Lett.* **2014**.[36] [f]From Lórenz-Fonfría et al. *J. Chem. Phys.* **2014**. [g]Nack et al. *FEBS Lett.* **2009**.[37] [h]From Lórenz -Fonfría et al. *Proc. Natl. Acad. Sci. U.S.A.* **2013**. [i]From Kato et al. *Nature* **2012**.[14] For ChR1 and ChR2, the values determined for ChR1 from *C. augustae* (*Ca*CR1) and ChR2 from *C. reinhardtii* (*Cr*ChR2) are shown, respectively. [j]n.d.: not determined.

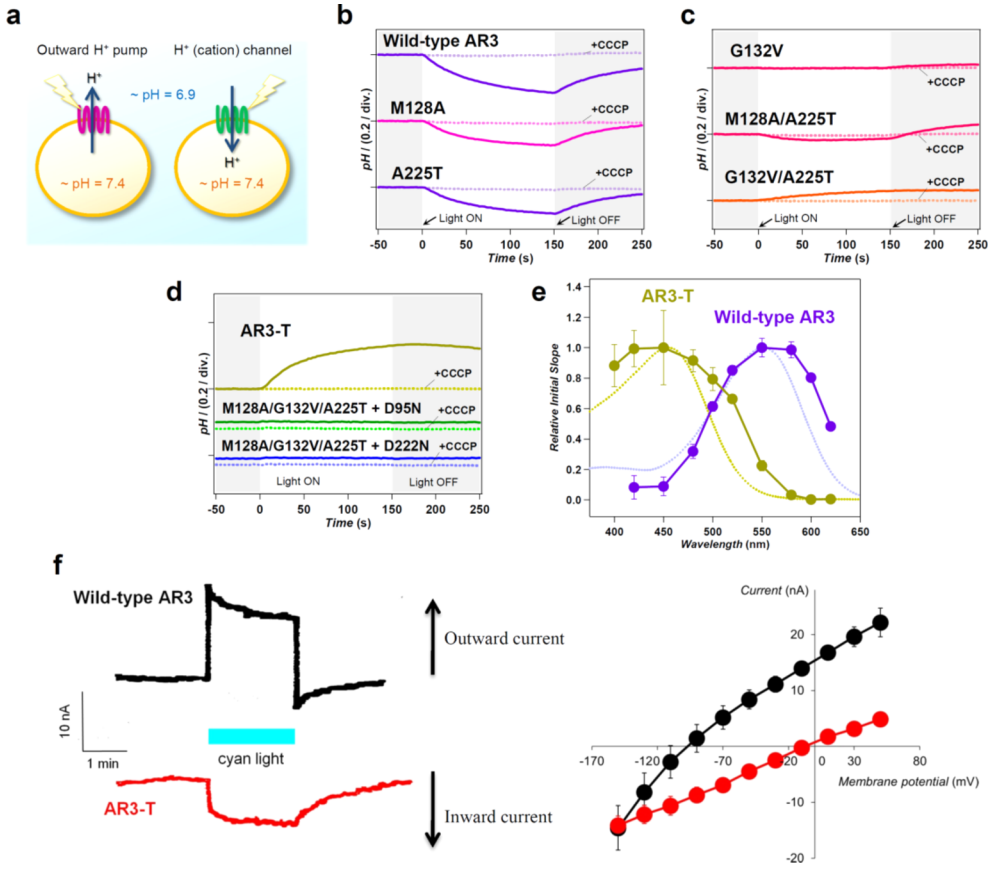

Figure 2. Ion transport activity of wild-type AR3 and its mutants. (a) Schematics of the experimental condition to measure the ion transport activity of the cells expressing proton pumps (left) and proton channels (right). (b–d) Light-induced pH change of wild-type AR3 and M128A, A225T (b), G132V, M128A/A225T and G132V/A225T (c), AR3-T, AR3-T plus D95N and AR3-T plus D222N (d). (e) Action spectra of the initial slopes of wild-type AR3 and AR3-T. Values are normalized at the peak values of each spectrum. (f) Photoinduced currents at −50 mV clamp voltage (left) and its *I*–*V* curves of oocytes expressing wild-type AR3 (black) and AR3-T (red).

70% ATR (see Table 1).[29,36−38] As shown in Figure 1f, the fraction of ATR in AR3-T was estimated to be 65%, which is similar to that in ChRs. Thus, the basic photochemical properties, absorption and retinal configuration, of AR3-T in the dark state were close to those of ChRs in the dark. The obtained λ_{max} and the retinal composition are summarized in Table 1 and Supporting Information Table S1. The quantities for the M128A/G132V mutant could not be measured because of difficulty in sample preparation due to its instability. Except for the M128A/G132V mutant, all mutations did not affect the levels of protein expression, as judged both by the color of cells and the amount of purified proteins.

Ion Transport Activities of the Color-Tuned AR3. Next we investigated the ion transport activity of wild-type AR3 and the mutants by monitoring the light-induced pH change of the suspension of *E. coli* cells expressing the corresponding proteins. In this experimental condition, the internal and external pH of the cells was kept at ~7.4 and ~6.9, respectively, by controlling the medium composition (Figure 2a). Therefore, in the case of wild-type AR3 representing outward H^+ pumping, the proton is transported to the external solvent and the pH of the solvent is expected to decrease upon light illumination. In fact, the wild-type AR3 and some of the mutants showed light-induced acidification of the external medium (Figure 2b). The

DOI: 10.1021/ja511788f
J. Am. Chem. Soc. 2015, 137, 3291−3299

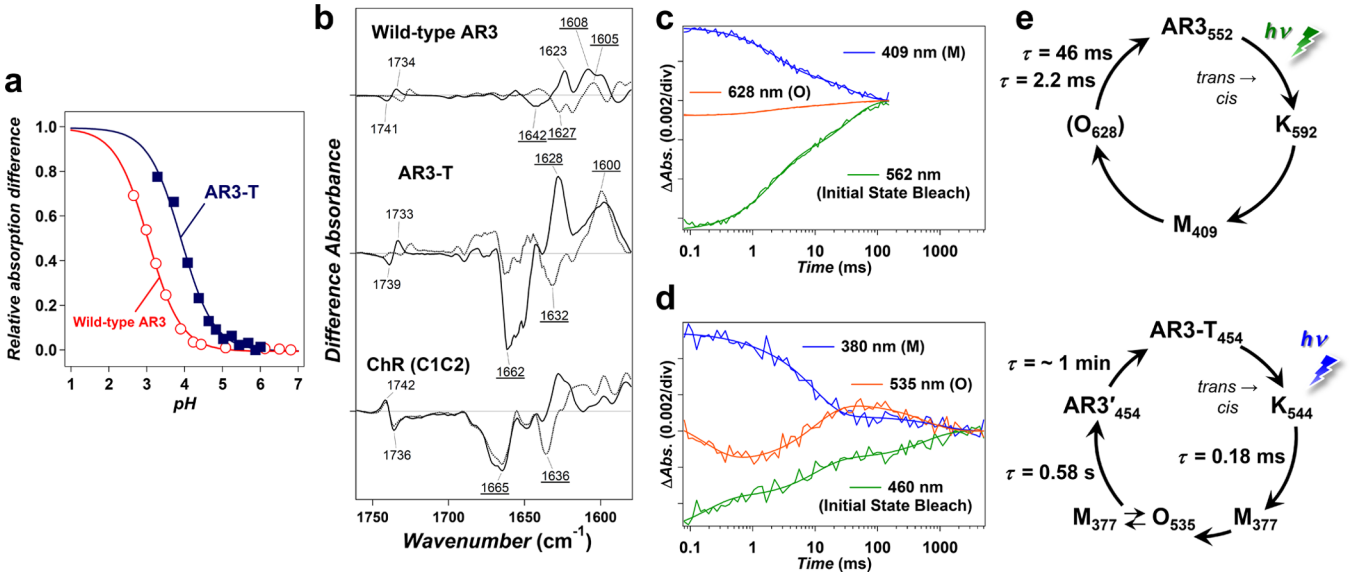

Figure 3. Photochemical and structural properties of wild-type AR3 and AR3-T. (a) pH-induced absorbance change of wild-type AR3 (○) and AR3-T (■). Solid lines are the fitted curves with the Henderson−Hasselbalch function; the pK_a values are listed in Table 1. (b) Difference FTIR spectra of wild-type AR3 (upper), AR3-T (middle), and the chimeric ChR (C1C2) (lower, reproduced from ref 15) at 77 K in the 1760−1580 cm^{-1} region. The solid and dotted lines are the spectra of the films hydrated with H_2O and D_2O, respectively. The underlined peaks correspond to C=N stretching vibrations of the Schiff base. (c, d) Time-evolution of transient absorption change of wild-type AR3 (c) and AR3-T (d) at specific wavelengths. The smooth lines are the fitting curves with a multiexponential function for the results (noisy lines). (e) Models for photocycles determined by flash photolysis experiments (c, d) for wild-type AR3 (upper) and AR3-T (lower). The lifetimes were determined by multiexponential fitting. Subscribed numbers indicate the absorption maxima of each state. The wavelengths of M and O intermediates were obtained from the spectra in Supporting Information Figure S3. The absorption spectrum of AR3′ is identical with the initial state, and the absorption maxima of K-intermediates were evaluated as explained in Supporting Information (Figure S2).

signal intensity decreased in the presence of an H^+-selective ionophore, CCCP, because the proton motive force collapsed (Figure 2b). These results suggest that wild-type AR3 and some of the mutants work as light-driven H^+ pumps across the cellular membrane.

On the other hand, only a small signal was observed for the G132V, M128A/A225T, and G132V/A225T mutants, indicating their weak H^+ transport activity (Figure 2c). This weak activity might be caused by a change(s) of some photochemical properties such as an abnormal pK_a change during the photoreaction cycle (photocycle). In contrast, light-induced alkalization of the external medium was observed for AR3-T (Figure 2d). The positive signal also disappeared in the presence of CCCP, suggesting inward H^+ transport. Thus, AR3-T produced a sufficiently robust response to permit the measurement of its action spectrum. For this, excitation light was monochromated by using interference filters with various center wavelengths, and the initial slope, representing the "proton transporting activity", was plotted against excitation wavelength (Figure 2e). The action spectrum of AR3-T blue-shifted by about 100 nm compared to that of wild-type AR3, and matches well with the shift in absorption between AR3-T and wild-type AR3 (dotted lines in Figure 2e). The good agreement between the action spectra and absorption ones confirms the fidelity of our quantification of proton transporting activity.

The inward H^+-transport of AR3-T raises two possibilities, a "light-driven inward H^+ pump" and a "light-gated H^+-permeable channel". The former actively transports H^+ at any membrane potential, while the latter passively transports H^+ and should be tightly coupled with membrane potential. To reveal whether AR3-T is an inward H^+ pump or an H^+-permeable channel, we expressed wild-type AR3 and AR3-T in oocyte cells and measured the photocurrent under different membrane potentials. Here we employed a cyan LED light source (~505 nm) because it can activate both wild-type AR3 and AR3-T with approximately similar efficiency (see Figure 2e). At a physiologically negative membrane potential (clamped voltage of −50 mV), a light-induced outward current was observed for wild-type AR3 while AR3-T showed a light-induced inward current (Figure 2f, left panel). These results are consistent with the H^+ transport assay experiments with *E. coli* cells (Figure 2b,d). The membrane potential was then changed to obtain *I*−*V* curves (Figure 2f, right panel). Wild-type AR3 showed a light-induced outward current over a wide range of membrane potentials, from −90 to +50 mV, indicating active ion transportation. In contrast, the direction of the light-induced current was inverted for AR3-T at a membrane potential of near 0 mV, and an outward current was observed at a positive membrane potential. These results clearly indicate that AR3-T works as a light-gated H^+ channel.

Photochemical and Structural Properties of the AR3 Variant Converted into a Channel. AR3-T provides an opportunity to identify photochemical and structural properties necessary to transport ions for ion channels by comparing with those of wild-type AR3, ChR, and BR. It is well-known that the salt bridge between the Schiff base lysine (Lys226 for AR3) and two aspartate residues (Asp95 and Asp222 for AR3) is essential for biological functions. In fact, neutralization of the residue disrupts ion transport activity both of ion pumps and ion channels.[1,39−41] To confirm this, an additional mutation was introduced into AR3-T. As shown in Figure 2d, light-induced ion transporting activity was not observed for the quadruple mutants having a replacement of D95N or D222N, indicating

DOI: 10.1021/ja511788f
J. Am. Chem. Soc. 2015, 137, 3291−3299

the functional importance of the counterions. In order to further investigate the property of the Schiff base region, pH-titration of the proteins was carried out to estimate the pK_a of the primary counterion Asp95 in AR3. The pK_a values were estimated by analysis with a single Henderson−Hasselbalch equation and resulted in a value of 3.0 for wild-type AR3 and a value of 3.9 for AR3-T (Figure 3a). The pK_a values for BR and C1C2 are 2.7 and 5.8, respectively.[14,42] These results suggest that the environment around the Schiff base in AR3-T becomes more hydrophobic than that of archaeal ion pumps which would be important for ion channel activity.

The structure of wild-type AR3 and AR3-T and their structural changes upon formation of the early intermediate (K) were investigated by FTIR spectroscopy (Figure 3b). Formation of the K-intermediate was confirmed by vibrational frequencies of C═C and C—C stretching (abbreviated as str hereafter) modes. The difference FTIR spectrum of wild-type AR3 was almost identical to that reported thus far[43] (Figure 3b and Supporting Information Figure S1). For AR3-T, *trans*−*cis* photoisomerization was confirmed by a spectral shift of the C—C str vibration of the retinal chromophore from 1199(−) to 1191(+) cm^{-1} (Supporting Information Figure S1). The C═C str vibrational bands for wild-type AR3 and AR3-T appeared at 1532(−)/1523(+) cm^{-1} and 1570(−)/1539(+) cm^{-1}, respectively. This is consistent with a well-known correlation between the frequency of the C═C str band and λ_{max} of the pigment (Supporting Information Figure S2).[44] The hydrogen out-of-plane (HOOP) modes of AR3-T resemble those of C1C2 rather than wild-type AR3, indicating similar structural changes between AR3-T and C1C2 (Supporting Information Figure S1). In the >1700 cm^{-1} region, where C═O str vibrations of the protonated-carboxylic acid appear, a 1741(−)/1734(+)-cm^{-1} band was observed for wild-type AR3; a similar band was also observed for AR3-T at 1739(−)/1731(+) cm^{-1} (Figure 3b). Since the 1740(−)/1733(+) cm^{-1} band was assigned to Asp115 for BR,[39] these results suggest that the hydrogen bonding of Asp125, corresponding to Asp115 of BR, strengthens upon formation of the K-intermediate both in wild-type AR3 and AR3-T. In contrast, it weakens in C1C2 (1736(−)/1742(+) cm^{-1}), suggesting that the alteration in hydrogen bonding of the Asp residue is not essential for functional differentiation. In the 1600−1700 cm^{-1} region where the C═N str of the Schiff base appears, a large difference was observed between wild-type AR3 and AR3-T. The bands that shifted between H_2O and D_2O were assigned to retinal C═N str vibrations (underlined peaks in Figure 3b). It is well-known that the difference in frequency ($\Delta\nu_{C=N}$) between H_2O and D_2O is positively correlated with the strength of the hydrogen bond of the Schiff base nitrogen. The $\Delta\nu_{C=N}$ of the unphotolyzed state of wild-type AR3 was 15 cm^{-1} which is similar to BR ($\Delta\nu_{C=N}$ = 13 cm^{-1}). In contrast, it was 30 cm^{-1} for AR3-T which is similar to those of ChRs (23−29 cm^{-1}, Table 1). As shown in Table 1, ion pumps and ion channels show relatively small and large isotope effects of the C═N stretching vibration, respectively, indicating that a strong hydrogen bond between the protonated retinal Schiff base and its counterion are important for the ion channels.

We also studied the photocycles by flash photolysis experiments. As shown in Figure 3c, wild-type AR3 showed only the M-intermediate in the time region of t > 100 μs in the current conditions (1 M NaCl, 50 mM Tris-Cl (pH 7)) and could be recovered to the initial state with the process being well-reproduced by a double-exponential function (τ = 2.2 and 46 ms) (Figure 3c,e). The K intermediate is expected to be present ahead of M as in other microbial rhodopsins. As expected, the FTIR measurement indicates the accumulation of a red-shifted intermediate assignable to K intermediate at 77 K (Figure 3b). Furthermore, the O intermediate should sequentially appear after M. However, its decay was faster than the decay of M, and the amount of accumulation was kinetically negligible (Supporting Information Figure S3). The photocycle of wild-type AR3 is summarized in Figure 3e. On the other hand, recovery of the initial state of AR3-T was much slower than wild-type AR3 (Figure 3d,e). In addition, a significant amount of O-accumulation was observed for AR3-T at t > 10 ms and around λ = 535 nm (Supportying Information Figure S3). Decay of the K-intermediate was observed for AR3-T (which is clear as a positive peak at 550 nm at t = 40 μs in Figure 3d that disappears at t = 770 μs), and the lifetime was estimated to be 0.18 ms. Then, following the decay of M (τ = 10 ms), the O intermediate, equilibrated with a trace amount of M, accumulated and decayed with a lifetime of 0.58 s. However, the photoinduced current of AR3-T remained for ∼1 min after light is turned off (Figure 2f). This indicates that channel closing is not coupled with the recovery of absorption of the retinal chromophore and that the channel continues to open for ∼1 min after the recovery of the change in absorption. We refer to this state as AR3′. The overall photocycle of AR3-T is depicted in Figure 3e. In general, ion pumps and ion channels show a relatively rapid and slow photocycling rate, respectively (see Table 1). Ion pumps have been optimized by nature to be furnished with fast photocycles because one ion is transported during a single photocycle. On the other hand, ChRs show slower photocycle compared to ion pumps.[45,46] The slower photocycle of AR3-T seems to somewhat resemble to that of ChR. However, the channel closing of ChR (e.g., 10 ms for *Cr*ChR2[45]) is much faster than that of AR3-T (∼1 min). Of note, some variants of ChR with long-lived open-state were reported to date.[22,47,48] For instance, C128T mutant of ChR2 shows 200-times long-lived open state.[47] In this case, the disruption of hydrogen bond between Cys128 and Asp156 leads to the long-lived open state. Because the cysteine residue is not conserved in AR3 and replaced by a Thr residue (Thr100), long-lived opening of AR3-T indicates the similarity of opening mechanism with the ChR2 C128T mutant. Thus, three substitutions around the retinal chromophore that alter the temporal behavior of the photocycle as well as the structure around the chromophore converted a light-driven H^+ pump into an light-gated H^+ channel. However, it is obvious that the transport efficiency of AR3-T is much lower than that of ChRs. In the case of the ChRs, hundreds of ions are transported upon the opening of one ChR molecule.[11,17] In contrast, the photoinduced current of AR3-T is comparable to or slightly lower than that of wild-type AR3 over a wide range of membrane potentials (Figure 2f). Because H^+ pumping rhodopsins transport one H^+ upon single photoexcitation, it is roughly estimated that nearly one H^+ is transported by single AR3-T upon single cycle event. Thus, although the modification of the retinal binding pocket made it possible to produce a light-gated H^+ channel, the efficiency is still much lower than that of natural channel rhodopsins.

■ DISCUSSION

In this study, we succeeded in the functional conversion of an H^+ pump AR3 to an H^+ channel by replacing only three amino acid residues. Is this applicable to other H^+ pump rhodopsins?

DOI: 10.1021/ja511788f
J. Am. Chem. Soc. 2015, 137, 3291−3299

Phylogenic analysis indicates that H^+-pumping rhodopsins are categorized into two major groups, archaeal and eubacterial rhodopsins (Figure 1a). We applied similar substitutions to another representative archaeal H^+ pump, BR from *Haloquadratum walsbyi* (*Hw*BR)[29] and a eubacterial H^+ pump (*Gloeobacter* rhodopsin from *Gloeobacter violaceus*, GR).[49] The triple mutants of *Hw*BR (M126A/G130V/A225T) and GR (M158A/G162V/A256T) showed large spectral blue-shifts (80 and 66 nm from wild-type, respectively), although the shifts were slightly smaller than that of AR3 (98 nm) (Supporting Information Tables S2 and S3 and Figure S4). The triple mutants of *Hw*BR and GR were expressed in *E. coli* cells, and H^+-transport activities were assayed (Supporting Information Figure S4c,d). The triple mutant of *Hw*BR showed small but significant inward H^+-transport activity, similar to AR3-T (Supporting Information Figure S4c), while the GR triple mutant retained its outward H^+ pumping activity (Supporting Information Figure S4d). These results suggest that while the spectral blue-shifts were achieved by triple substitutions around retinal for both archaeal and eubacterial H^+ pumps, functional conversion can be evoked only for the archaeal H^+ pump (AR3 and *Hw*BR) and not for the eubacterial pump GR. Although their functions are similar, the sequential identities of amino acids are low (~20%) between archaeal and eubacterial rhodopsins.[1] We assumed that common structural element(s) for functional differentiation conserved between archaeal H^+-pumping rhodopsins and channel rhodopsins are lost in eubacterial rhodopsins, and further modification(s) are required to convert the eubacterial H^+ pump into an H^+ channel. Thus, we speculate that the ion channels evolved from archaeal H^+ pumps.

So far, functional conversions from a H^+ to a Cl^- pump,[24] from cation to anion channels[22,23] and from pump to sensor,[25] were achieved by the replacement of 1−3 amino acid(s) in microbial rhodopsin family proteins. The present study is the first demonstration of the conversion from a light-driven H^+ pump into a light-gated H^+ channel. Figure 4 shows schematic models for the ion pumping mechanism in wild-type AR3 (left) and the H^+ channeling mechanism in AR3-T (right). The position of the β-ionone ring of C1C2 retinal is located toward the cytoplasmic side more than the H^+ pump (Figure 1d).[13,14] We hypothesized that the position of the wild-type AR3 ring can be moved to a similar position to C1C2 by optimizing the size of the residues in upper (M128A) and lower (G132V) sides of the ring. Consequently, AR3-T became an H^+ channel with a blue-shifted absorption maximum by three substitutions. This supports our prediction that the position of the β-ionone ring is important both for function and color of ion transport machineries.

In a previous study, we replaced Ser151 on helix E to an alanine in addition to M128A and A225T for AR3 (M128A/S151A/A225T). In this case, although a 52 nm blue-shift was observed, the H^+ pump function was still maintained.[29] Quantum chemical calculations suggested that a β-ionone ring rotation occurred in the mutant. For the rotation of the ring, a structural perturbation of the retinal chromophore was mainly restricted in the ring region, but not in the polyene chain and the Schiff base region. On the other hand, the G132V mutant used in this study is expected to cause steric hindrance between the mutated residue and the ring region, resulting in alteration of the polyene chain and the Schiff base region. In fact, the larger pK_a of AR3-T suggests that the Schiff base region becomes more hydrophobic than wild-type AR3

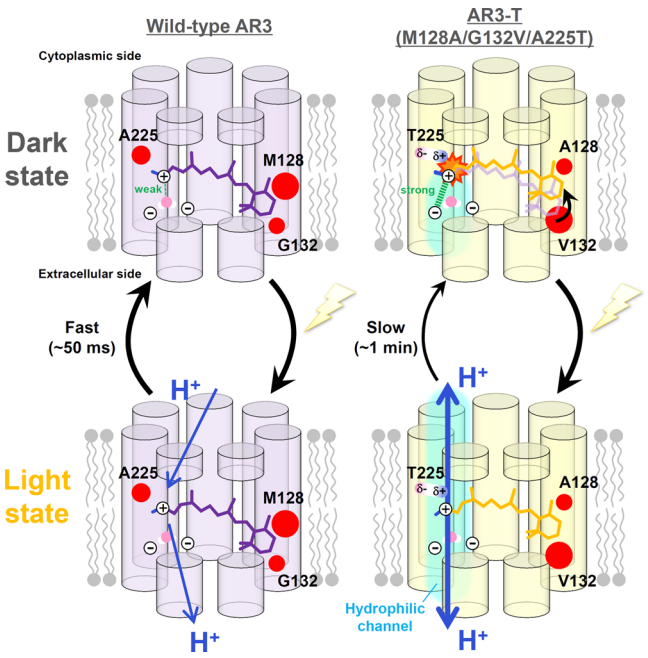

Figure 4. Schematic drawing of ion transport mechanism of wild-type AR3 and AR3-T. For wild-type AR3, H^+ is released from a carboxylic residue upon photoillumination, and then H^+ is taken up from the cytoplasmic side through a proton-donating residue. The H^+ pumping activity is facilitated by a fast photocycling rate (~50 ms) because one proton is transported to the extracellular side during a single photocycle. On the other hand, for AR3-T, the chromophore structure is modified by replacement of three amino acid residues (M128A, G132V, and A225T). The modifications lead to alteration both of the β-ionone ring region and the Schiff base one, resulting in an increase in hydrophilicity of the ion transport pathway. The H^+ channeling activity is facilitated by a slow photocycling rate (~1 min) because the protons are transported in the photointermediate(s).

(Figures 3a and 4). Furthermore, structural differences are also suggested from the increase in strength of the hydrogen bond of both the Schiff base and the fraction of ATR configuration. These structural alterations produce a water-accessible channel from the extracellular side, and this half channel would be connected to the cytoplasmic side upon activation by light (Figure 4, right lower panel). Thus, we speculate that H^+ transport occurs by the opening of this transient hydrophilic channel in which the direction of transport is determined according to the membrane potential and H^+ gradient. In ChRs the ion permeation pathway is estimated to be located between helices A−C and G, differently from the path for proton/ion pump in microbial rhodopsins including AR3.[14] Where proton permeation occurs is not clear in AR3-T, but the low currents (Figure 2f) suggest that proton permeation could be caused by a leak in the normal proton-pumping pathway (i.e., helices C, D, F, and G), as shown before for *Gloeobacter* rhodopsin in the acidic conditions.[50] From the results of current study together with other findings, we concluded that the functional determinant in ion channeling retinal proteins is localized at the center of the membrane-spanning domain, but not on the cytoplasmic and extracellular domains.

In addition to its biological significance, functional conversion will create a new way of rational design and engineering of retinal proteins that can be applied to optogenetics. Ion pumps and ion channels are utilized for

DOI: 10.1021/ja511788f
J. Am. Chem. Soc. 2015, 137, 3291−3299

neural silencing and activation, respectively. Therefore, AR3-T could be applied to neural activation as well as ChRs. The different absorption of AR3-T from that of the neural silencer wild-type AR3 makes it possible to control neural silencing and activation with different colors of light. Because AR3-T is easily expressed in *E. coli* cells, further modifications by a combination of intended and random mutagenesis are easier than for ChRs. It is known that ChR2 shows a reduction in the photocurrent after the maximum current immediately appears after light illumination, which is called desensitization. Of note, no desensitization was observed for the AR3-T mutant during illumination (Figure 2f). This would be suitable for the constant depolarization of cells to control neurons. However, the property of AR3-T is not sufficiently ideal for optogenetic application. It shows relatively slow off-function dynamics (~1 min) (Figure 2f), and blue-light excitation sometimes causes toxicity for the optical manipulation of cells and tissues.[51] To solve these problems, further engineering to develop variants similar to many optimized ones designed in the case of ChR2[52,53] might be required for AR3-T as well.

■ ASSOCIATED CONTENT

Supporting Information

Absorption maxima, opsin shifts, and retinal configurations of the wild-type AR3 and its mutants (Table S1). Absorption maxima, opsin shifts, retinal configurations and directions of the proton pumping of the wild-type *Hw*BR and the triple mutant (Table S2). Absorption maxima, opsin shifts, retinal configurations, and directions of the proton pumping of the wild-type GR and the triple mutant (Table S3). Difference FTIR spectra of wild-type AR3 and AR3-T (middle) and the chimeric ChR (C1C2) in 1595−850 cm^{-1} region (Figure S1). The correlation of the absorption maxima (λ_{max}'s) and the frequencies of retinal C=C stretching vibrations of microbial rhodopsins (Figure S2). Transient absorption spectra of wild-type AR3 and AR3-T in the *E. coli* membrane (Figure S3). The absorption spectra and proton transport activity of wild-type *Hw*BR, GR, and their mutants (Figure S4). This material is available free of charge via the Internet at http://pubs.acs.org.

■ AUTHOR INFORMATION

Corresponding Author

sudo@pharm.okayama-u.ac.jp

Notes

The authors declare no competing financial interest.

■ ACKNOWLEDGMENTS

This work was financially supported by grants from the Japanese Ministry of Education, Culture, Sports, Science, and Technology to KI (26708001, 26115706 and 26620005), KS (23790060), SM (23590062, 26460044), SH (25104004 and 25291034), HK (25104009) and to YSud (23687019 and 24121712).

■ REFERENCES

(1) Ernst, O. P.; Lodowski, D. T.; Elstner, M.; Hegemann, P.; Brown, L. S.; Kandori, H. *Chem. Rev.* **2014**, *114*, 126.

(2) Oesterhelt, D.; Stoeckenius, W. *Nat. New Biol.* **1971**, *233*, 149.

(3) Béjà, O.; Aravind, L.; Koonin, E. V.; Suzuki, M. T.; Hadd, A.; Nguyen, L. P.; Jovanovich, S. B.; Gates, C. M.; Feldman, R. A.; Spudich, J. L.; Spudich, E. N.; DeLong, E. F. *Science* **2000**, *289*, 1902.

(4) Inoue, K.; Ono, H.; Abe-Yoshizumi, R.; Yoshizawa, S.; Ito, H.; Kogure, K.; Kandori, H. *Nat. Commun.* **2013**, *4*, 1678.

(5) Matsuno-Yagi, A.; Mukohata, Y. *Biochem. Biophys. Res. Commun.* **1977**, *78*, 237.

(6) Yoshizawa, S.; Kumagai, Y.; Kim, H.; Ogura, Y.; Hayashi, T.; Iwasaki, W.; DeLong, E. F.; Kogure, K. *Proc. Natl. Acad. Sci. U.S.A.* **2014**, *111*, 6732.

(7) Inoue, K.; Tsukamoto, T.; Sudo, Y. *Biochim. Biophys. Acta* **2013**, *1837*, 562.

(8) Bogomolni, R. A.; Spudich, J. L. *Proc. Natl. Acad. Sci. U.S.A.* **1982**, *79*, 6250.

(9) Takahashi, T.; Tomioka, H.; Kamo, N.; Kobatake, Y. *FEMS Microbiol. Lett.* **1985**, *28*, 161.

(10) Nagel, G.; Ollig, D.; Fuhrmann, M.; Kateriya, S.; Musti, A. M.; Bamberg, E.; Hegemann, P. *Science* **2002**, *296*, 2395.

(11) Nagel, G.; Szellas, T.; Huhn, W.; Kateriya, S.; Adeishvili, N.; Berthold, P.; Ollig, D.; Hegemann, P.; Bamberg, E. *Proc. Natl. Acad. Sci. U.S.A.* **2003**, *100*, 13940.

(12) Jung, K. H.; Trivedi, V. D.; Spudich, J. L. *Mol. Microbiol.* **2003**, *47*, 1513.

(13) Luecke, H.; Schobert, B.; Richter, H. T.; Cartailler, J. P.; Lanyi, J. K. *J. Mol. Biol.* **1999**, *291*, 899.

(14) Kato, H. E.; Zhang, F.; Yizhar, O.; Ramakrishnan, C.; Nishizawa, T.; Hirata, K.; Ito, J.; Aita, Y.; Tsukazaki, T.; Hayashi, S.; Hegemann, P.; Maturana, A. D.; Ishitani, R.; Deisseroth, K.; Nureki, O. *Nature* **2012**, *482*, 369.

(15) Ito, S.; Kato, H. E.; Taniguchi, R.; Iwata, T.; Nureki, O.; Kandori, H. *J. Am. Chem. Soc.* **2014**, *136*, 3475.

(16) Martinez, A.; Bradley, A. S.; Waldbauer, J. R.; Summons, R. E.; DeLong, E. F. *Proc. Natl. Acad. Sci. U.S.A.* **2007**, *104*, 5590.

(17) Hegemann, P. *Annu. Rev. Plant. Biol.* **2008**, *59*, 167.

(18) Berthold, P.; Tsunoda, S. P.; Ernst, O. P.; Mages, W.; Gradmann, D.; Hegemann, P. *Plant Cell* **2008**, *20*, 1665.

(19) Boyden, E. S.; Zhang, F.; Bamberg, E.; Nagel, G.; Deisseroth, K. *Nat. Neurosci.* **2005**, *8*, 1263.

(20) Chow, B. Y.; Han, X.; Dobry, A. S.; Qian, X.; Chuong, A. S.; Li, M.; Henninger, M. A.; Belfort, G. M.; Lin, Y.; Monahan, P. E.; Boyden, E. S. *Nature* **2010**, *463*, 98.

(21) Gradinaru, V.; Thompson, K. R.; Deisseroth, K. *Brain Cell Biol.* **2008**, *36*, 129.

(22) Wietek, J.; Wiegert, J. S.; Adeishvili, N.; Schneider, F.; Watanabe, H.; Tsunoda, S. P.; Vogt, A.; Elstner, M.; Oertner, T. G.; Hegemann, P. *Science* **2014**, *344*, 409.

(23) Berndt, A.; Lee, S. Y.; Ramakrishnan, C.; Deisseroth, K. *Science* **2014**, *344*, 420.

(24) Sasaki, J.; Brown, L. S.; Chon, Y. S.; Kandori, H.; Maeda, A.; Needleman, R.; Lanyi, J. K. *Science* **1995**, *269*, 73.

(25) Sudo, Y.; Spudich, J. L. *Proc. Natl. Acad. Sci. U.S.A.* **2006**, *103*, 16129.

(26) Sudo, Y.; Yuasa, Y.; Shibata, J.; Suzuki, D.; Homma, M. *J. Biol. Chem.* **2011**, *286*, 11328.

(27) Shimono, K.; Ikeura, Y.; Sudo, Y.; Iwamoto, M.; Kamo, N. *Biochim. Biophys. Acta* **2001**, *1515*, 92.

(28) Mori, A.; Yagasaki, J.; Homma, M.; Reissig, L.; Sudo, Y. *Chem. Phys.* **2013**, *419*, 23.

(29) Sudo, Y.; Okazaki, A.; Ono, H.; Yagasaki, J.; Sugo, S.; Kamiya, M.; Reissig, L.; Inoue, K.; Ihara, K.; Kandori, H.; Takagi, S.; Hayashi, S. *J. Biol. Chem.* **2013**, *288*, 20624.

(30) Tsukamoto, T.; Inoue, K.; Kandori, H.; Sudo, Y. *J. Biol. Chem.* **2013**, *288*, 21581.

(31) Seki, A.; Miyauchi, S.; Hayashi, S.; Kikukawa, T.; Kubo, M.; Demura, M.; Ganapathy, V.; Kamo, N. *Biophys. J.* **2007**, *92*, 2559.

(32) Sudo, Y.; Okada, A.; Suzuki, D.; Inoue, K.; Irieda, H.; Sakai, M.; Fujii, M.; Furutani, Y.; Kandori, H.; Homma, M. *Biochemistry* **2009**, *48*, 10136.

(33) Kandori, H.; Shimono, K.; Sudo, Y.; Iwamoto, M.; Shichida, Y.; Kamo, N. *Biochemistry* **2001**, *40*, 9238.

(34) Tanimoto, T.; Furutani, Y.; Kandori, H. *Biochemistry* **2003**, *42*, 2300.

(35) Kandori, H.; Kinoshita, N.; Shichida, Y.; Maeda, A. *J. Phys. Chem. B* **1998**, *102*, 7899.

DOI: 10.1021/ja511788f
J. Am. Chem. Soc. 2015, 137, 3291−3299

(36) Muders, V.; Kerruth, S.; Lorenz-Fonfria, V. A.; Bamann, C.; Heberle, J.; Schlesinger, R. *FEBS Lett.* **2014**, *588*, 2301.
(37) Nack, M.; Radu, I.; Bamann, C.; Bamberg, E.; Heberle, J. *FEBS Lett.* **2009**, *583*, 3676.
(38) Ihara, K.; Amemiya, T.; Miyashita, Y.; Mukohata, Y. *Biophys. J.* **1994**, *67*, 1187.
(39) Braiman, M. S.; Mogi, T.; Marti, T.; Stern, L. J.; Khorana, H. G.; Rothschild, K. J. *Biochemistry* **1988**, *27*, 8516.
(40) Marinetti, T.; Subramaniam, S.; Mogi, T.; Marti, T.; Khorana, H. G. *Proc. Natl. Acad. Sci. U.S.A.* **1989**, *86*, 529.
(41) Lanyi, J. K. *Annu. Rev. Physiol.* **2004**, *66*, 665.
(42) Brown, L. S.; Bonet, L.; Needleman, R.; Lanyi, J. K. *Biophys. J.* **1993**, *65*, 124.
(43) Clair, E. C.; Ogren, J. I.; Mamaev, S.; Kralj, J. M.; Rothschild, K. J. *J. Biol. Phys.* **2012**, *38*, 153.
(44) Aton, B.; Doukas, A. G.; Callender, R. H.; Becher, B.; Ebrey, T. G. *Biochemistry* **1977**, *16*, 2995.
(45) Lórenz-Fonfría, V. A.; Resler, T.; Krause, N.; Nack, M.; Gossing, M.; Fischer von Mollard, G.; Bamann, C.; Bamberg, E.; Schlesinger, R.; Heberle, J. *Proc. Natl. Acad. Sci. U.S.A.* **2013**, *110*, E1273.
(46) Lórenz-Fonfría, V. A.; Muders, V.; Schlesinger, R.; Heberle, J. *J. Chem. Phys.* **2014**, *141*, 22D507.
(47) Stehfest, K.; Ritter, E.; Berndt, A.; Bartl, F.; Hegemann, P. *J. Mol. Biol.* **2010**, *398*, 690.
(48) Lin, J. Y.; Lin, M. Z.; Steinbach, P.; Tsien, R. Y. *Biophys. J.* **2009**, *96*, 1803.
(49) Miranda, M. R.; Choi, A. R.; Shi, L.; Bezerra, A. G., Jr.; Jung, K. H.; Brown, L. S. *Biophys. J.* **2009**, *96*, 1471.
(50) Vogt, A.; Wietek, J.; Hegemann, P. *Biophys. J.* **2013**, *105*, 2055.
(51) Hockberger, P. E.; S, T. A.; Centonze, V. E.; Lavin, C.; Chu, S.; Dadras, S.; Reddy, J. K.; White, J. G. *Proc. Natl. Acad. Sci. U.S.A.* **1999**, *96*, 6255.
(52) Lin, J. Y.; Knutsen, P. M.; Muller, A.; Kleinfeld, D.; Tsien, R. Y. *Nat. Neurosci.* **2013**, *16*, 1499.
(53) Prigge, M.; Schneider, F.; Tsunoda, S. P.; Shilyansky, C.; Wietek, J.; Deisseroth, K.; Hegemann, P. *J. Biol. Chem.* **2012**, *287*, 31804.

DOI: 10.1021/ja511788f
J. Am. Chem. Soc. 2015, 137, 3291−3299